MARFE Stability Analysis in ELMy H-mode NSTX Plasmas

F. Kelly
Unaffiliated
R. Maqueda
Nova Photonics
R. Maingi
Oak Ridge National Lab
and the NSTX Research Team

48th APS-DPP Meeting
Oct. 30-Nov. 3, 2006
Philadelphia, PA

Abstract

The temperature and density dependence of plasma and atomic processes have been previously identified as the cause of many transition phenomena in tokamaks, e.g. Multifaceted Asymmetric Radiation From the Edge (MARFE). In the National Spherical Torus Experiment (NSTX), edge-localized modes (ELMs) are observed using a fast-framing camera to interact with an inner-wall MARFE, leading to partial burn-through of the MARFE during the ELM cycle.[1] After the ELM pulse, light pattern subsequently transitions from a helical pattern (a residual from the previous partially burned-through MARFE) to the classic asymmetric MARFE pattern, with the cycle being repeated at each ELM. We use thermal instability theory to attempt an explanation of the MARFE/ELM dynamics in NSTX. In particular a single discharge provides many examples of plasma profiles which are thermally stable and unstable. Details of the analysis are presented.

[1] R. Maqueda, et al., NO1.00013 this conference

Introduction

- Large or Type I ELMs direct a substantial fraction of the plasma stored energy to the plasma-facing components (PFCs).
- The resulting erosion of PFCs over many pulses and the redistribution of the eroded material are critical issues that will affect the performance and operation of ITER or the proposed spherical torus (ST) concept for a Component Test Facility (CTF).
- The fast-evolving structure of MARFEs and ELMs is observed in NSTX using a Nova Photonics fast-framing camera.
- We apply basic thermal instability theory to assess interactions between MARFEs and ELMs in NSTX.
- The goal is a physics-based model and understanding to use in extrapolation for next generation ST and in ITER.

Type V ELM filament imaged in the edge of NSTX shot #119318

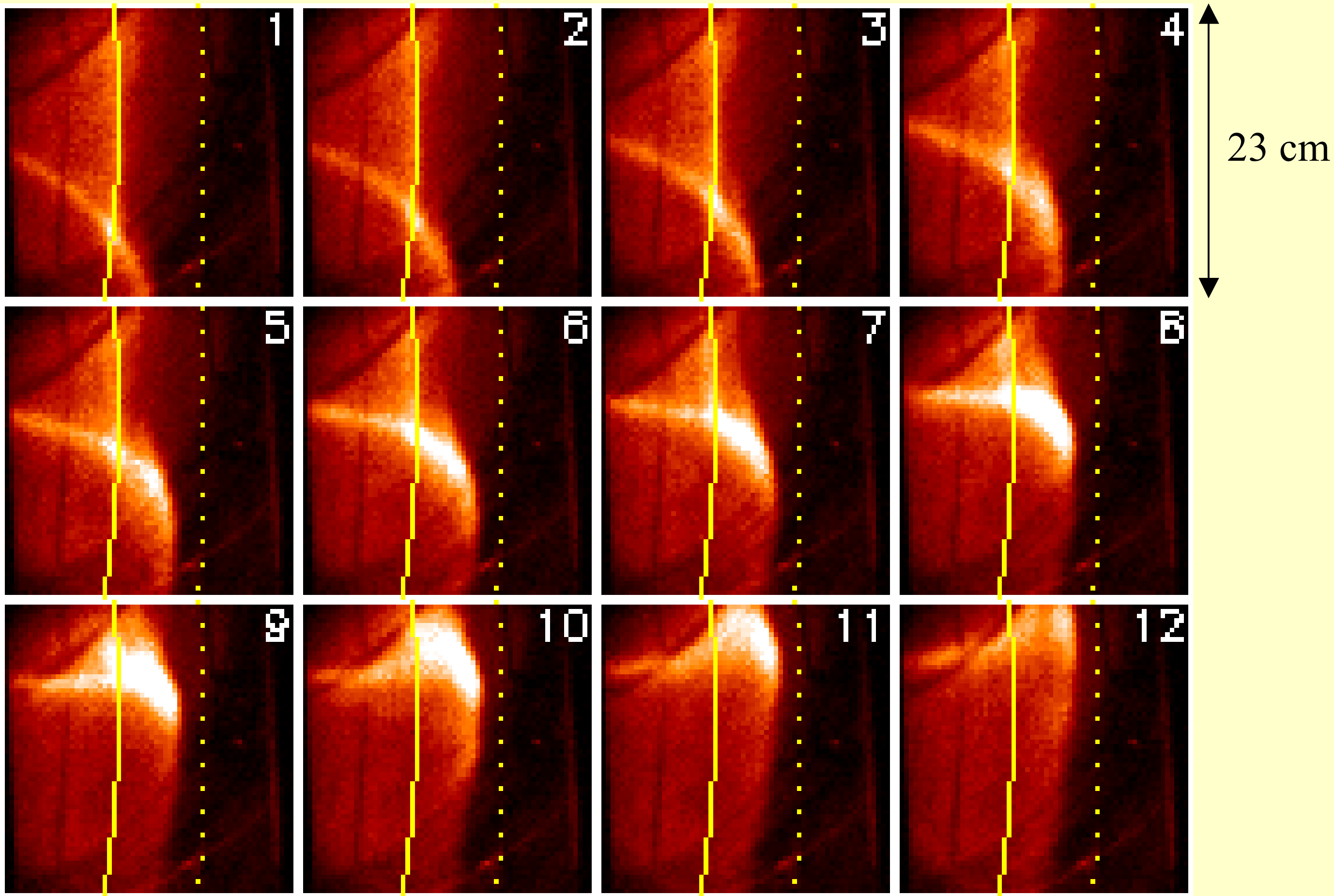

Sequence imaged in D_α light (3 μs exposures at 120000 frames/s). Separatrix is indicated by solid yellow line and antenna limiter shadow by dotted line. Filament moves poloidally from the bottom left corner (#1 at 668.343 ms) to top of image (#12 at 668.434 ms).
Maqueda, et al., O-37, PSI-17 (2006) submitted to JNM

Type V ELM filament structure

- Observed in shot 119318 (800kA, 6.5MW NBI, Lower Single Null) to be well aligned with local magnetic field
- One or two ionization front “ribbons” move upward poloidally and in counter-Ip direction toroidally (~8 km/s)
- Ribbon is displaced by ~4 cm from the main D_α emission layer, the radial width of the ribbon, $v_r < 0.2$ km/s
- Ribbon extends ~13 cm poloidally of which only the outer ionizing edge is seen in D_α emission
- Type V ELM ribbon maybe momentarily outward shifted magnetic flux surface Maqueda, et al., O-37, PSI-17 (2006)

Hot, dense ELM filaments lose particles and energy to nearby closed field lines inside separatrix and hence to MARFE

MARFE evolution in high-density NSTX shot #117125

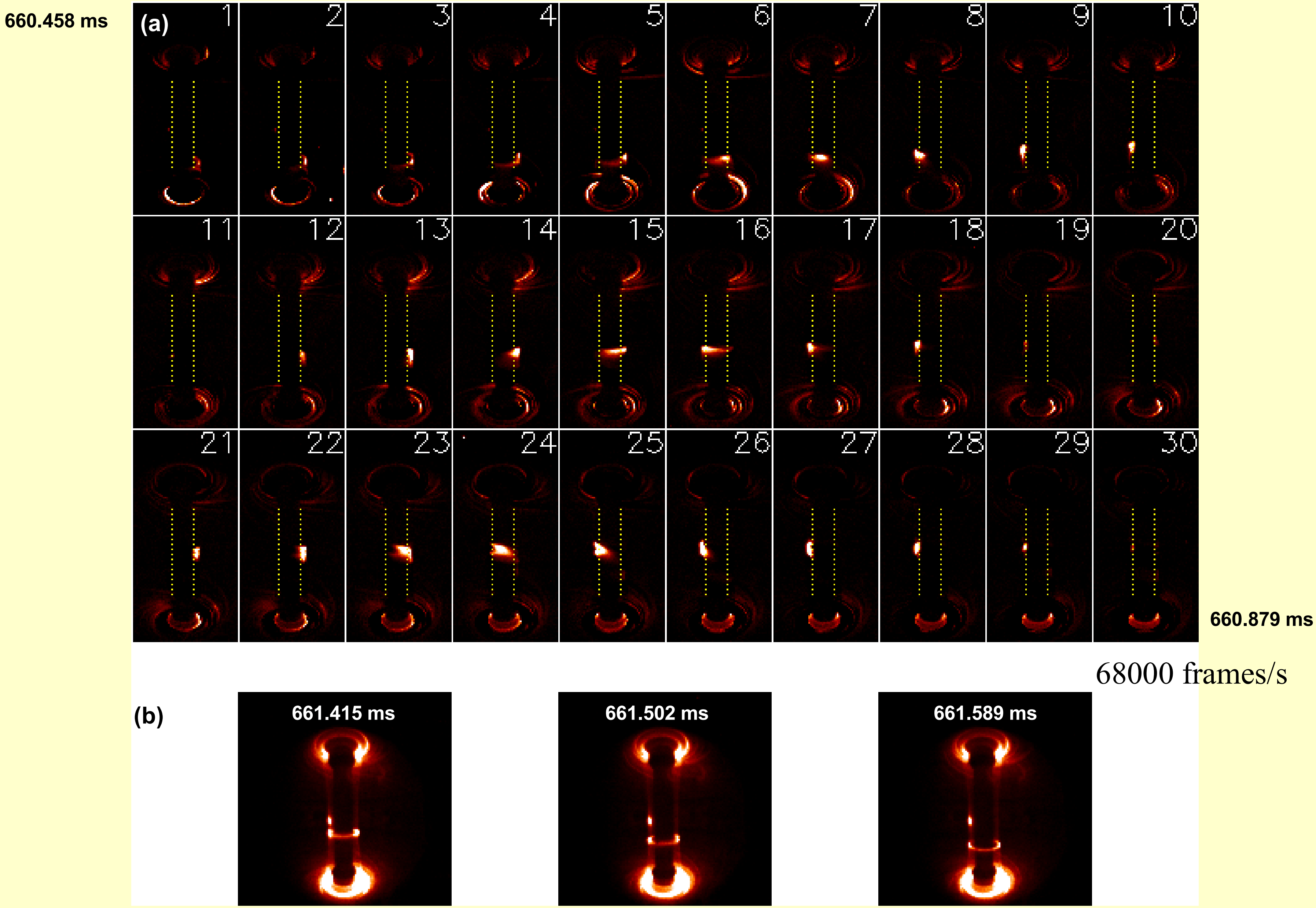

MARFE/ELM dynamics observed in NSTX shot #117125 (800 kA, 6.0 MW, Double Null)

- Poloidally and toroidally localized MARFE remnant (plasmoid) moves upward following magnetic field line
- Plasmoid (MARFE precursor) upward movement stagnates and expands into a toroidally symmetric ring
- MARFE ring moves downward in ion ∇B drift direction
- ELM activity in divertor region coincides with burn through of most of MARFE

- Type I ELM (at ~665.5 ms) burns through MARFE

Downward ion grad-B drift places stable MARFE position near lower divertor. Asakura, et al., NF 36, 795(1996)
Slight upper null bias places stagnation point near upper divertor.

ELM cycle drives dynamics of MARFE, remnant and precursor

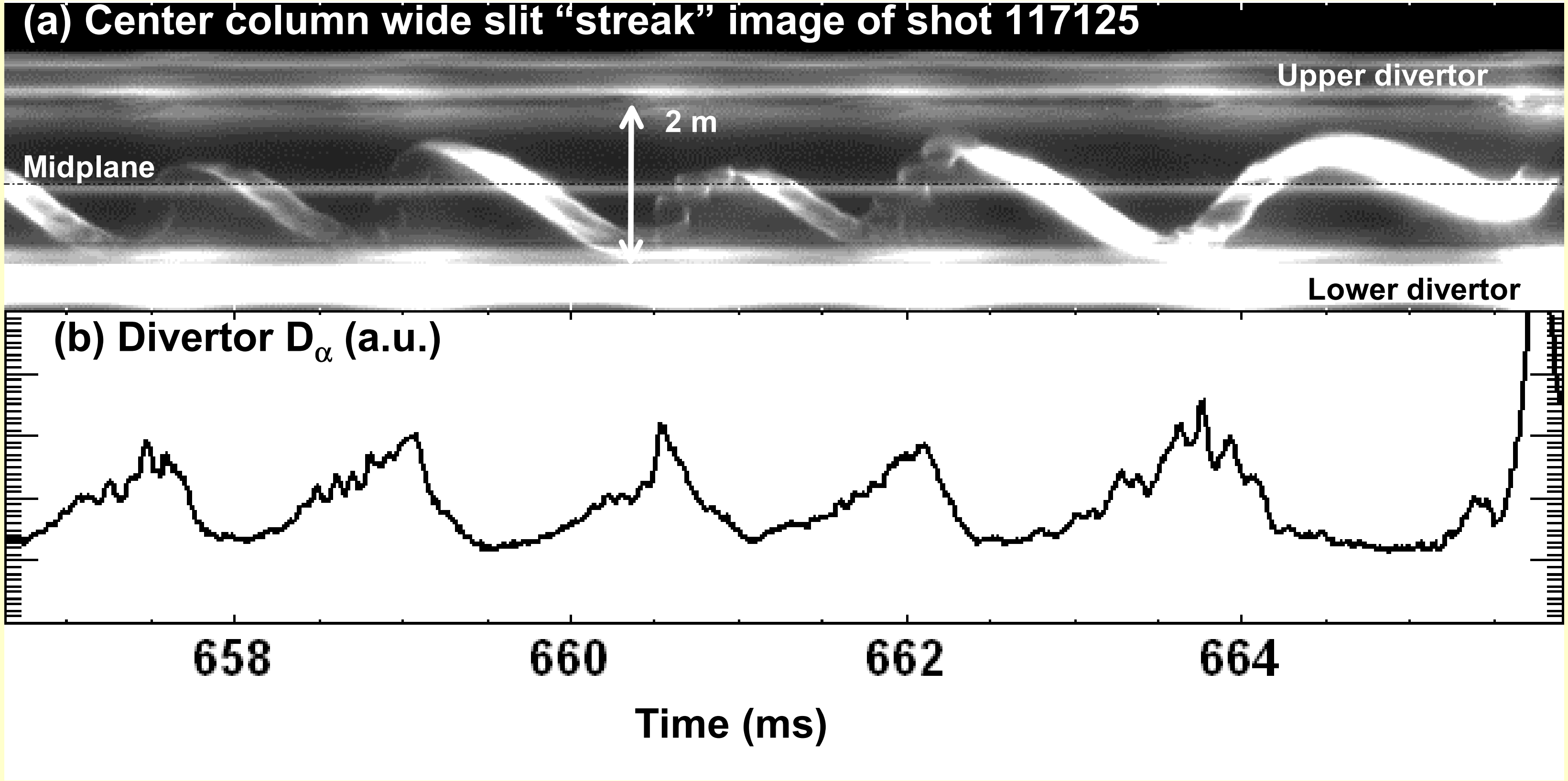

ELM cycle and MARFE cycle are closely linked, however, periods and lengths vary. Precursor of Type I ELM reverses MARFE movement and then burns through MARFE.

Basic MARFE theory

- Drake PF **30** (1987) found the MARFE to be a radiative condensation instability governed by the following linearized equation.

parallel and perpendicular conduction radiative condensation

$$\frac{5}{2} n\gamma\tilde{T} + k_{\parallel}^{2}\kappa_{\parallel}\tilde{T} - \kappa_{\perp}\frac{\partial^{2}\tilde{T}}{\partial r^{2}} = nn_{z}\ \frac{2L_{z}}{T} - \frac{\partial L_{z}}{\partial T}\ \tilde{T} \qquad (1)$$

- Wesson and Hender NF **33** (1993) observed that the most unstable mode varies as cos θ and wave number $k_{\parallel} = 1/qR$

$$\kappa_{\perp}\frac{\partial^{2}\tilde{T}}{\partial r^{2}} - k_{\parallel}^{2}\kappa_{\parallel}\tilde{T} = nn_{z}T^{2}\frac{\partial}{\partial T}\left(\frac{L_{z}(T)}{T^{2}}\right)\tilde{T} \qquad (2)$$

- Mahdavi, et al. 24th EPS (1997) and Maingi and Mahdavi, FST **48** (2005), incorporated non-equilibrium radiation effect of neutrals in a uniform edge distribution, but neglected perpendicular conduction and atomic cooling to obtain an equation that is equivalent to

$$n_{marfe} \leq \sqrt{\frac{\left(\kappa_{0}/Z_{eff}\right)T^{1/2}/(qR)^{2}}{-\sum_{z} f_{z}\frac{\partial}{\partial T}\left(\frac{L_{z}(T,f_{0})}{T^{2}}\right)}} \qquad (3)$$

Mahdavi, et al. 24th EPS (1997) and Maingi and Mahdavi, FST **48** (2005), used an assumed a neutral fraction of $f_0 = 0.001$ together with measured impurity concentrations of 1% carbon and 0.06% oxygen for two DIII-D shots: 89525 with $q_{95} = 9$ which marfed and 90323 with q95 = 3.2 which reached twice the Greenwald density without a MARFE. Defining the MARFE Index

$$MI \equiv \frac{n_{exp}}{n_{marfe}}$$

Eq. (3) results in $MI = 3.1\text{x}10^{19}/2.94\text{x}10^{19} = 1.05$ for shot 89525 and $MI = 3.4\text{x}10^{19}/3.87\text{x}10^{20} = 0.088$ for shot 90323. Stacey, Phys. Plasmas **9**, 2692 (2002) found shot 90323 at the MARFE threshold (MI = 1) by 2000ms, however the density continued to rise until a radiative collapse occurred at 2260 ms.

Application of Eq. (3) to the TEXTOR power scan series of shots analyzed in Kelly, Stacey, Rapp, and Brix, Phys. Plasmas **8**, 3382 (2001) resulted in a predicted MARFE density which exceeded the measured edge density by factor of ~3,as shown in the following slide.

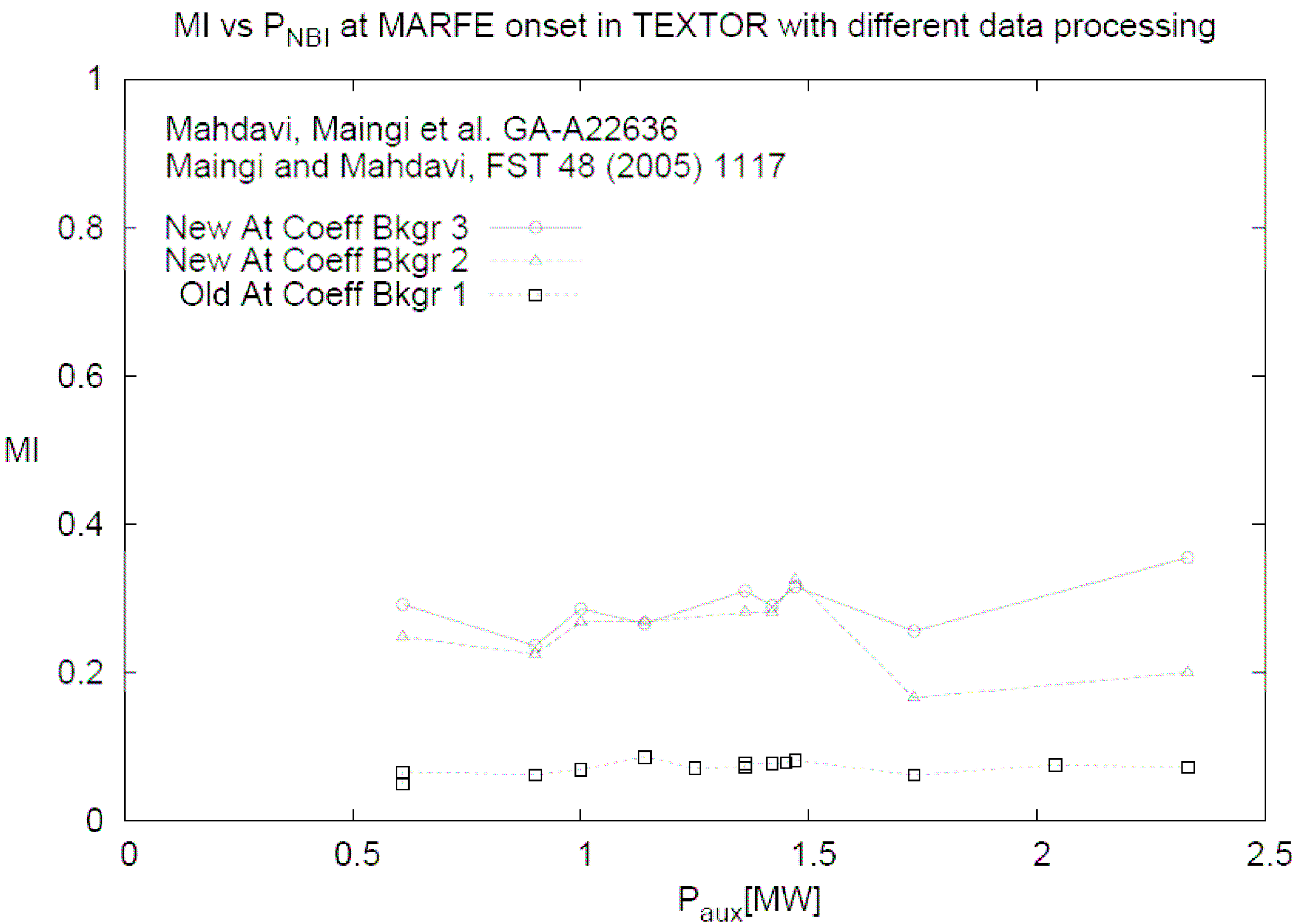
MI vs P_NBI at MARFE onset in TEXTOR with different data processing
Mahdavi, Maingi et al. GA-A22636
Maingi and Mahdavi, FST 48 (2005) 1117
New At Coeff Bkgr 3
New At Coeff Bkgr 2
Old At Coeff Bkgr 1
MI
0
0.2
0.4
0.6
0.8
1
0
0.5
1
1.5
2
2.5
P_aux[MW]

Table 1 MARFE stability calculation for Eq. (3), Mahdavi et al., 24th EPS (1997), for f_0=10-3 and f_z=2x10-2, 5x10-2 at estimated Ψ_N = 0.992 normalized poloidal flux for NSTX discharge 117125

TS times (sec)	Condition	R (m)	T_e(TS)[a] (eV)	n_e(TS)[a] (m-3)	n_{marfe}[b] (m-3)	MI[b]	n_{marfe}[c] (m-3)	MI[c]
0.326662	no marfe	1.3977	64.3	2.24E+19	3.08E+20	0.073	1.72E+20	0.130
0.343345	no marfe	1.3942	129.4	3.87E+19	1.39E+21	0.028	7.50E+20	0.052
0.359992	no marfe	1.3951	61.5	2.25E+19	2.74E+20	0.082	1.54E+20	0.146
0.376685	upward move	1.3934	27.4	1.99E+19	3.41E+19	0.583	1.95E+19	1.022
0.393332	no marfe	1.4247	15.3	7.46E+18	1.07E+19	0.700	6.07E+18	1.229
0.410015	no marfe	1.4170	27.5	8.92E+18	3.39E+19	0.263	1.93E+19	0.461
0.426662	no marfe	1.4251	10.1	2.00E+18	6.58E+18	0.304	3.86E+18	0.519
0.443345	no marfe	1.3984	117.6	3.77E+19	1.19E+21	0.032	6.44E+20	0.059
0.459992	no marfe	1.4180	26.5	9.90E+18	3.12E+19	0.318	1.78E+19	0.557
0.476685	birth	1.4251	22.2	1.71E+19	2.14E+19	0.799	1.22E+19	1.400
0.493322	stagnation	1.4254	12.7	5.93E+18	8.28E+18	0.716	4.76E+18	1.246
0.510025	stagnation	1.4155	39.5	1.67E+19	8.46E+19	0.197	4.84E+19	0.345
0.526662	no marfe	1.4248	23.0	1.20E+19	2.29E+19	0.524	1.31E+19	0.919
0.543345	birth	1.4183	20.3	7.87E+18	1.77E+19	0.446	1.01E+19	0.780
0.559992	no marfe	1.4247	12.3	5.71E+18	7.99E+18	0.715	4.60E+18	1.242
0.576685	no marfe	1.4178	25.4	1.40E+19	2.85E+19	0.491	1.62E+19	0.862
0.593332	birth	1.4145	39.8	1.15E+19	8.57E+19	0.134	4.90E+19	0.235
0.610025	no marfe	1.4167	28.5	9.34E+18	3.69E+19	0.253	2.11E+19	0.443
0.626662	burn	1.4262	18.8	9.33E+18	1.53E+19	0.611	8.72E+18	1.070
0.643355	stagnation	1.4278	24.8	1.09E+19	2.69E+19	0.405	1.53E+19	0.711
0.660002	move down	1.4292	39.9	1.60E+19	8.68E+19	0.184	4.96E+19	0.323
0.676685	stable at top	1.4304	104.1	3.15E+19	9.49E+20	0.033	5.16E+20	0.061
0.693332	no marfe	1.4555	35.0	8.85E+18	6.12E+19	0.145	3.50E+19	0.253
0.710015	birth	1.4495	68.1	1.63E+19	3.55E+20	0.046	1.98E+20	0.082
0.726662	birth	1.4303	22.8	1.08E+19	2.24E+19	0.481	1.28E+19	0.844
0.743355	no marfe	1.4253	12.9	3.28E+18	8.34E+18	0.393	4.78E+18	0.686
0.759992	no marfe	1.4160	53.9	2.67E+19	1.95E+20	0.137	1.10E+20	0.243
0.776685	no marfe	1.3937	109.6	3.86E+19	1.05E+21	0.037	5.70E+20	0.068
0.793332	no marfe	1.3944	111.3	3.86E+19	1.08E+21	0.036	5.86E+20	0.066
0.810015	stagnation	1.3888	55.1	2.56E+19	2.06E+20	0.124	1.16E+20	0.220

a Thomson Scattering T_e and n_e interpolated to the estimated (LRDFIT04) position of 99.2% poloidal flux surface with connection length, L_c = 40 m.
b n_{marfe} and MI = n_e/n_{marfe} with a carbon impurity fraction of 0.02 and L_c = 40 m.
c n_{marfe} and MI = n_e/n_{marfe} with a carbon impurity fraction of 0.05 and L_c = 40 m.

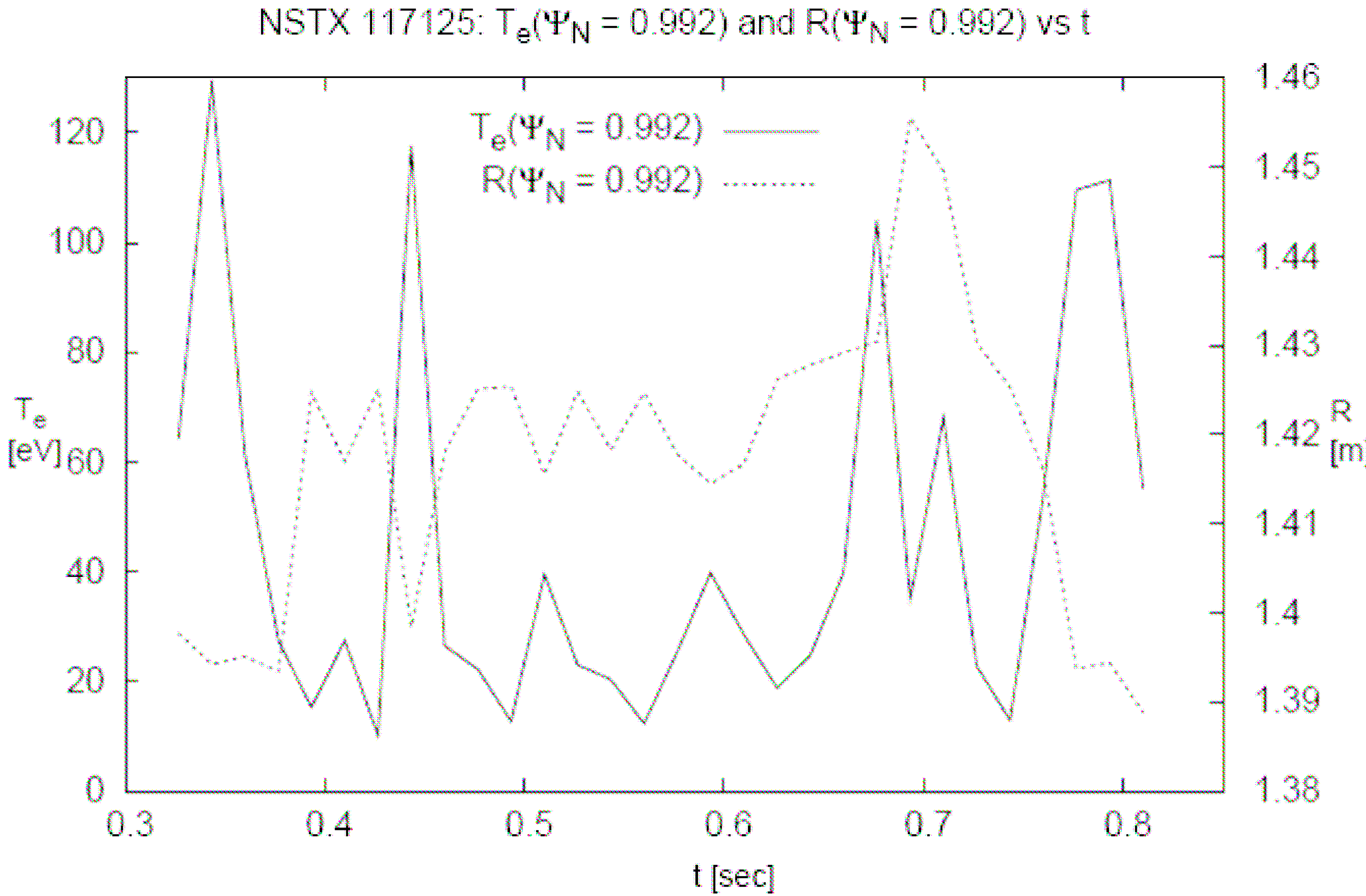
NSTX 117125: $T_e(\Psi_N = 0.992)$ and $R(\Psi_N = 0.992)$ vs t
$T_e(\Psi_N = 0.992)$
$R(\Psi_N = 0.992)$
T_e [eV]
R [m]
t [sec]
0
20
40
60
80
100
120
1.38
1.39
1.4
1.41
1.42
1.43
1.44
1.45
1.46
0.3
0.4
0.5
0.6
0.7
0.8

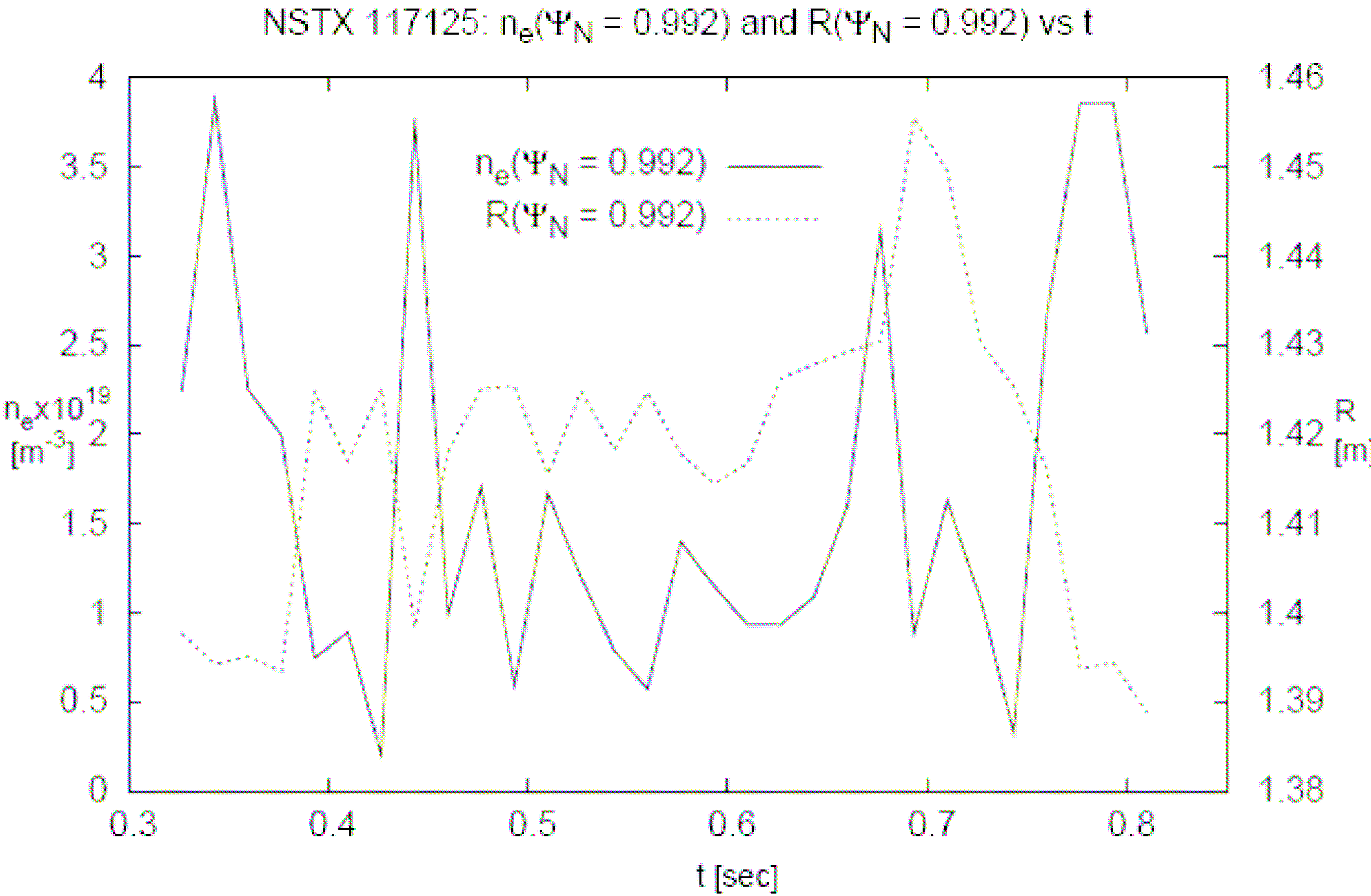
NSTX 117125: $n_e(\Psi_N = 0.992)$ and $R(\Psi_N = 0.992)$ vs t
$n_e(\Psi_N = 0.992)$
$R(\Psi_N = 0.992)$
$n_e x10^{19}$ [m^{-3}]
R [m]
t [sec]
0
0.5
1
1.5
2
2.5
3
3.5
4
1.38
1.39
1.4
1.41
1.42
1.43
1.44
1.45
1.46
0.3
0.4
0.5
0.6
0.7
0.8

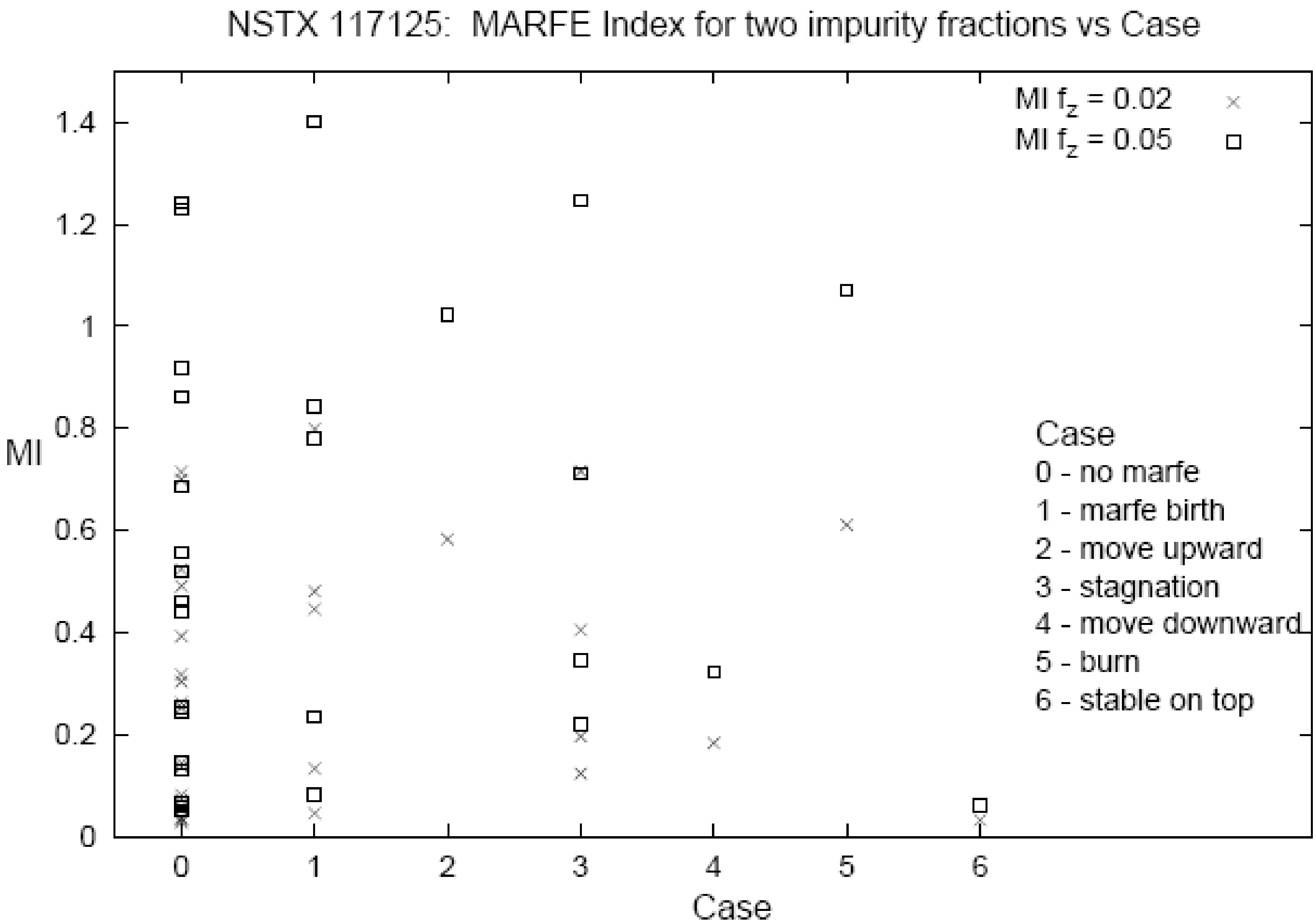
NSTX 117125: MARFE Index for two impurity fractions vs Case
MI f_z = 0.02
MI f_z = 0.05
Case
0 - no marfe
1 - marfe birth
2 - move upward
3 - stagnation
4 - move downward
5 - burn
6 - stable on top
MI
Case
0
0.2
0.4
0.6
0.8
1
1.2
1.4
0
1
2
3
4
5
6

Cases: center image is nearest to TS time, left -72.5 µs, right +72.5 ms

0 = no marfe; t = 0.326662 s

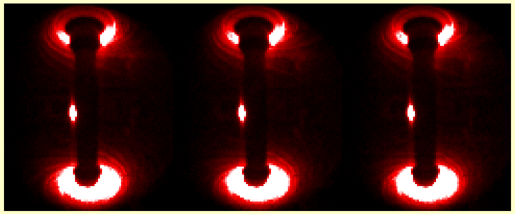

3 = stagnation; 0.493322 s

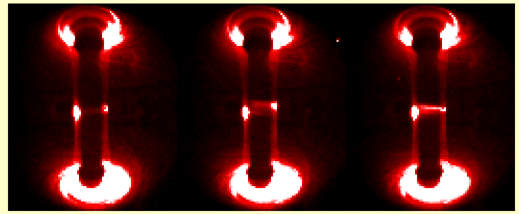

6 = stable at top; 0.676685 s

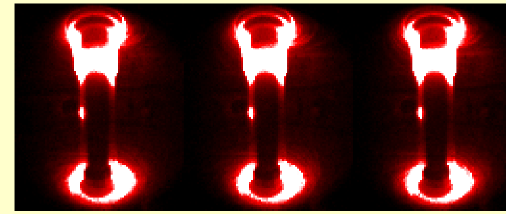

1 = marfe birth; 0.726662 s

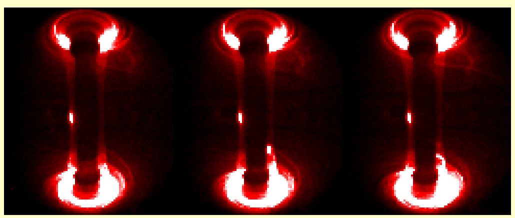

4 = move down; 0.660002 s

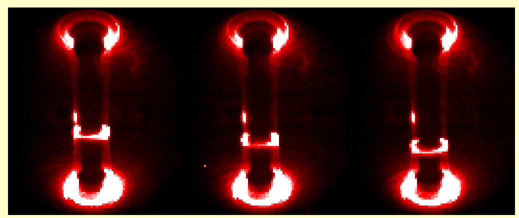

2 = move up; 0.376685 s

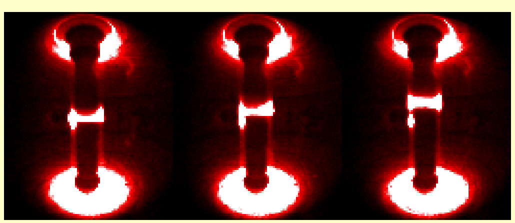

5 = burn; 0.626662 s

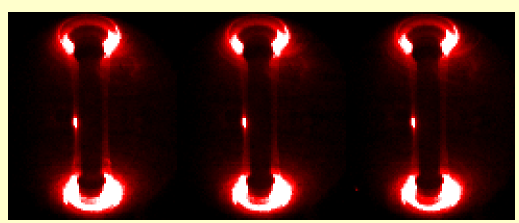

Discussion of Results

- Type V ELMs in NSTX are elongated filaments that rotate counter I_p , NBI and plasma rotation with lifetimes of 0.5-1.0 ms.
- ELM filaments are ribbon-like, wider cross-field than radially.
- ELM filament propagates radially shifting the ionization front and probably the magnetic flux surfaces as well.
- ELM releases pulse of heat and particles inside the separatrix affecting MARFE movement.
- A MARFE is born, in some cases, from a precursor resulting from a partial burn-through of the preceding MARFE.
- The MARFE remnant/precursor moves up the center stack, while the newly born MARFE moves down.
- Uncertainty in the location of the separatrix cause the comparison of basic MARFE theory with experiment to be inconclusive.

Conclusions

- Heat pulse from the ELM within the closed magnetic flux surface causes the burn-through of the MARFE and subsequent parallel flux causes the upward movement of the plasmoid.
- Location of stagnation point may depend on the timing and amount of particle and energy flux during the ELM event.
- Independent of vertical location of stagnation, downward movement occurs at a constant speed (uniform between cycles) governed by ion grad-B drift.
- Better estimate of separatrix location, and temporal and spatial resolution of Thomson Scattering measurements are needed to compare observation with more advanced theories.
- Critical analysis of terms important to MARFE and plasmoid, stability and movement necessary.
- Further theoretical development may require 3-D or 2-D analysis due to inherent non-axisymmetry of MARFE/ELM interaction.

Further analysis of MARFE/ELM dynamics

Perform a linear stability analysis on NSTX data using the theories of W. M. Stacey, beginning with the simplest version 2-D (||, r) that includes parallel conduction and atomic physics: Plasma Phys. Control. Fusion **39**, 1245 (1997) and Fusion Technol. **36**, 38 (1999).

$$n_{\max}\left(k_{\|}\right)=\left[\chi_{\|}k_{\|}^{2}+\chi_{r}\left(\nu L_{T}^{-2}-\left(1-C^{(2)}\right)L_{n}^{-1}L_{T}^{-1}\right)\right]\div\left\{f_{z}\left[\left(\nu+1-C^{(2)}\right)\frac{L_{z}}{T}-\frac{\partial L_{z}}{\partial T}\right]\right. \quad (4)$$

$$\left.+f_{0}\left[\frac{E_{ion}\langle\sigma v\rangle_{ion}}{T}\left(\upsilon-\frac{T}{\langle\sigma v\rangle_{ion}}\frac{\partial\langle\sigma v\rangle_{ion}}{\partial T}\right)\right]+f_{0}^{cold}\left[\frac{3}{2}\langle\sigma v\rangle_{at}\left(\nu-1-\frac{T}{\langle\sigma v\rangle_{at}}\frac{\partial\langle\sigma v\rangle_{at}}{\partial T}\right)\right]\right\}$$

Simulate dynamics of MARFE/ELM interaction with 2-D or 3-D model, e.g.

Continuity eqs.:

plasma particles: $$\frac{\partial n}{\partial t}+\nabla_{\|}\left(nV_{\|}\right)+\nabla_{\perp}\Gamma_{\perp}=k_{ion}^{H}n\left(n_{H}^{0}+n_{H}^{*}\right)-k_{rec}^{H}n^{2}$$

recycling hydrogen neutrals: $$\nabla_{\perp}\Gamma_{H}^{0}=-\left(k_{cx}^{H}+k_{ion}^{H}\right)nn_{H}^{0}+k_{rec}^{H}n^{2}$$

charge-exchange hydrogen neutrals: $$\nabla_{\perp}\Gamma_{H}^{*}=k_{cx}^{H}nn_{H}^{0}-k_{ion}^{H}nn_{H}^{*}$$

Parallel momentum eq.:

$$\frac{\partial m_i n V_\parallel}{\partial t} + \nabla_\parallel (2nT) + \nabla_\perp \left[-D_\perp \nabla_\perp (n) m_i V_\parallel \right] = -m_i V_\parallel \nabla_\perp \Gamma_H^*$$

Heat eq.:

$$3\frac{\partial nT}{\partial t} + \nabla_\parallel \left(-\kappa_\parallel \nabla_\parallel T + 5nV_\parallel T \right) + \nabla_\perp q_\perp + \nabla_\vartheta q_d = -k_{ion}^H n n_H E_i - Q_{rad}^I$$

Particle and heat fluxes $\perp$**B**:

$$\Gamma_\perp = -D_\perp \nabla_\perp n + n\,\mathrm{v}_\mathrm{r}, \quad q_\perp = -\kappa_\perp \nabla_\perp T + 3\Gamma_\perp T$$

$$q_d = \frac{5cn}{2eB}\left[\frac{\vec{B}}{B(\vartheta)} \times \left(T_i \nabla T_i - T_e \nabla T_e \right) \right]$$

M. Z. Tokar, Phys. Plasma **10**, 4378 (2003), Phys. Plasmas **12**, 052510 (2005).